Time evolution of the electric field using the rapid expansion method with pseudospectral evaluation of spatial derivatives — Part 1

Time evolution of the electric field using the rapid expansion method (REM) with pseudo-spectral evaluation of spatial derivatives Part I

Paul L. Stoffa[1] and Anton Ziolkowski[2]

Paper submitted to *Geophysics* 2 March 2018

Revised paper submitted 11 April 2019

[1]University of Texas at Austin, Institute for Geophysics and Department of Geological Sciences, Jackson School of Geosciences, Austin, Texas, U.S.A.
Email: stoffa@ig.utexas.edu

[2]University of Edinburgh, School of Geosciences, Edinburgh, United Kingdom.
Email: anton.ziolkowski@ed.ac.uk

ABSTRACT

We present a method for modeling transient EM data acquired on land or at sea. The 3D three-component time response of the electric wave field is simulated by considering the spatial and temporal responses separately and employing numerical methods best suited for each. Here we use the rapid expansion method to develop the three-component electric wave field time response from the spatial responses found using a pseudo-spectral method. The results are free of numerical dispersion and accurate to the Nyquist frequency in time and space. The resulting diffusive field is a weighted sum of Chebyshev polynomials, which exhibit a wave-like character and are very sensitive to small perturbations in the medium. The method is intrinsically parallel which leads to computational efficiency. Numerical results compare favorably with the analytic response and 1D methods even though the computations are innately 3D.

INTRODUCTION

Low frequency electromagnetic (EM) modeling in conducting media has become especially important in the last ten years during which there has been a rapid development of the controlled source electromagnetic (CSEM) method. The method was originally developed for use in academic research in deep water (>500m) to study the conductivity of the Earth's crust (Cox, 1981). It employs a continuous periodic signal containing a few discrete frequencies emitted by a horizontal current dipole source towed about 50m above the seafloor, and receiver nodes on the seafloor which measure two orthogonal horizontal electric field components and three orthogonal magnetic field components (Sinha et al., 1990). Commercialization of this system for the detection of hydrocarbon reserves in deep water was first described by Eidesmo et al. (2002) and Ellingsrud et al. (2002). The technique has now become an accepted tool in the de-risking of expensive deep water exploration wells with more than 50 deep water wells drilled based on the results of CSEM data (Hesthammer et al., 2010).

An alternative approach is to use a transient source signal with a broad frequency bandwidth (Edwards & Chave, 1986). This method also employs a horizontal electric dipole source and an array of in-line electric field receivers and has been applied in the investigation of shallow methane gas (Schwalenberg et al. 2005). The transient approach has also been commercialized (Ziolkowski et al., 2008) and applied successfully in detecting hydrocarbons in shallow water (Ziolkowski et al., 2010), within a fully towed system (Anderson & Mattsson, 2010), and on land (Wright et al., 2002; Ziolkowski et al., 2007).

Unlike the seismic method, there is no ray-theory for EM, and interpretation of the data is totally dependent on modeling. Flexible 3D three-component full-bandwidth modeling is therefore important in CSEM for survey design and especially for inversion of the data. Mittet (2010) provides an excellent overview of finite-difference time-domain approaches to the problem of modeling EM data and analyzes the trade-off between speed and accuracy before

proposing his own improved finite-difference approach. All finite-difference schemes, however, have accuracy limited by the approximations of the spatial and temporal derivatives.

Druskin and Knizhnerman (1994) developed an explicit three-dimensional solver for the diffusion of electromagnetic fields in arbitrarily heterogeneous conductive media, based on a global Krylov subspace (Lanczos) approximation of the solution in the time and frequency domains. Carcione (2006) introduced a Chebyshev algorithm which we use in this paper. Carcione (2006) remarked, 'Both the Krylov and Chebyshev algorithms . . . are highly efficient explicit algorithms. The advantage of the Chebyshev method over the Krylov approach is that it does not use inner products. This feature makes the Chebyshev algorithm highly attractive in parallel computing.'

We solve for the 3D three-component electric field (E-field) directly using an explicit time evolution called the rapid expansion method (REM), proposed by Tal-Ezer (1986, 1989), combined with a pseudo-spectral evaluation for the spatial derivatives (Fornberg, 1987; Fornberg, 1988). Our method is based on the approach proposed by Carcione (2006), who solved the 2D problem for a magnetic source. Pestana and Stoffa (2010) have applied REM to the time evolution of the 3D acoustic wave equation. Unlike finite difference methods, this method is accurate to the Nyquist frequency in time and the Nyquist wavenumber in a homogeneous wholespace. Further, the method is unconditionally stable. We incorporate the analytic solution for an impulsive electric dipole source in a full space as our initial condition to begin the time evolution of the 3D three-component E-field.

The REM expands the exponential of the spatial operator using Chebyshev polynomials which are then integrated with weights derived from a modified Bessel function. Displays of the Chebyshev polynomials exhibit a wave-like character that shows where the energy is propagating. After the integration of the polynomials with the modified Bessel function weights the diffuse character of the energy becomes obvious.

We first present the derivation of the algorithm, closely following the notation of Carcione (2006). Then we compute the result for a dipole buried in a whole space and compare it with the analytical solution to demonstrate the accuracy of the method. Finally, we show a 3D example where the wave-like character of the Chebyshev polynomials is demonstrated and removal of the effects of the direct (and, where necessary the air) wave from the E-field data is proposed.

THE METHOD

We discuss the modeling of three-component 3D CSEM data using an approach based on Carcione (2006). This involves the calculation of Chebyshev polynomials as a way to obtain an accurate but intermediate representation of the electromagnetic wave field in space. We closely follow the development and notation of Carcione (2006), but we extend Carcione's two dimensional (x,z) analysis for dipole magnetic sources to three dimensions (x,y,z) for an electric dipole source.

Theory

The electric field vector $\mathbf{E}(x,y,z,t)$ satisfies the diffusion equation

$$\frac{\partial \mathbf{E}}{\partial t} = -\frac{1}{\mu\sigma}\nabla\times\nabla\times\mathbf{E} - \frac{1}{\sigma}\frac{\partial \mathbf{J}}{\partial t} \quad , \tag{1}$$

in which $\mu = \mu_0 = 4\pi 10^{-7}$ H/m is the magnetic permeability, σ(S/m) is the electrical conductivity, which is the reciprocal of the resistivity, and **J** is the current source. Equation 1 is of the form

$$\frac{\partial \mathbf{w}}{\partial t} = \mathbf{G}\mathbf{w} + \mathbf{s}\,, \tag{2}$$

where **w** is the wavefield (and could be the electric or the magnetic field), **s** is the source term, and, for the 3D case,

$$\mathbf{G} = -\frac{1}{\mu\sigma}\nabla\times\nabla = -\frac{1}{\mu\sigma}\begin{pmatrix} -\left(\partial_y^2+\partial_z^2\right) & \partial_y\partial_x & \partial_z\partial_x \\ \partial_x\partial_y & -\left(\partial_x^2+\partial_z^2\right) & \partial_z\partial_y \\ \partial_x\partial_z & \partial_y\partial_z & -\left(\partial_x^2+\partial_y^2\right) \end{pmatrix}. \tag{3}$$

After discretization the solution of equation 2, satisfying the initial condition $\mathbf{w}(0) = \mathbf{w}_0$, is formally given by (Carcione 2006, equation 18) as

$$\mathbf{w}_N(t) = \exp(t\mathbf{G}_N)\mathbf{w}_N^0 + \int_0^t \exp(\tau\mathbf{G}_N)\mathbf{s}_N(t-\tau)d\tau\,, \tag{4}$$

where N is the number of gridpoints, $\mathbf{w}_N^0$ is the initial field and $\mathbf{s}_N(t)$ represents a spatial distribution of time-dependent sources. For a single impulsive source at $t = 0$ we may use the wavefield at $t = 0^+$, just after the impulse, as an initial field condition. Using the Chebyshev expansion of $\exp(x)$, in the absence of sources, the discrete solution (Carcione 2006) is

$$\mathbf{w}_N^M(t) = \sum_{k=0}^{M} b_k(t)T_k(\mathbf{F}_N)\mathbf{w}_N^0\,, \tag{5}$$

where

$$\mathbf{F}_N = \frac{1}{b}\left(\mathbf{G}_N + b\mathbf{I}\right), \tag{6}$$

I is the identity matrix of dimension 3 and b is the absolute value of the eigenvalue of matrix $\mathbf{G_N}$ having the largest negative real part (See Carcione, 2006 for a more detailed discussion). Here

$$b_k(t) = c_k \exp(-bt) I_k(bt), \tag{7}$$

$c_0 = 1$, $c_k = 2$ for $k \geq 1$, and I_k is the modified Bessel function.

The value of $T_k(\mathbf{F}_N)\mathbf{w}_N^0$ is computed using the recurrence relation for Chebyshev polynomials (Abramowitz and Stegun, 1972 and Carcione 2006). To simplify the notation we let $\mathbf{Q}_k$ represent the kth Chebyshev polynomial

$$\mathbf{Q}_k = T_k(\mathbf{F}_N)\mathbf{w}_N^0. \tag{8}$$

Hence,

$$\mathbf{Q}_k = 2\mathbf{F}_N\mathbf{Q}_{k-1} - \mathbf{Q}_{k-2}, \quad k \geq 2, \tag{9}$$

$$\mathbf{Q}_0 = \mathbf{w}_N^0, \quad \mathbf{Q}_1 = \mathbf{F}_N\mathbf{w}_N^0, \tag{10}$$

and

$$\mathbf{w}_N^M(t) = \sum_{k=0}^{M} b_k(t)\mathbf{Q}_k \ . \tag{11}$$

The maximum wavenumber components are the Nyquist wavenumbers, which for grid spacings Δx, Δy and Δz are $k_x = \pi/\Delta x$, $k_y = \pi/\Delta y$ and $k_z = \pi/\Delta z$. Hence, the value of b is

$$b = \frac{\pi^2}{\mu\sigma_{min}}\left(\frac{1}{\Delta x^2} + \frac{1}{\Delta y^2} + \frac{1}{\Delta z^2}\right), \tag{12}$$

where $\sigma_{\min}$ is the lowest value of conductivity in the model and b has units of s^{-1}. As Tal-Ezer (1989, equation 4.13) shows, the polynomial order should be $O(\sqrt{bt})$. Carcione (2006) found that

$$M = \beta\sqrt{bt} \tag{13}$$

is sufficient to obtain stability and accuracy, with β in the range 5 to 6.

Implementation

This numerical formulation for the time advance of the electric wave field lends itself to a fast computational solution with no required changes or approximations that reduce accuracy or introduce numerical dispersion. The main computational component is a 3D fast Fourier transform (FFT), which is now readily available for both single core and parallel machine architectures. Further, the problem itself can be organized as three independent computations, one for each component, and carried out in parallel. Within each independent calculation of the

individual components, further parallelization is possible for their work developing that component's updated response. We use Message-Passing Interface (MPI) for the parallelization of the three independent *E* wave field components and Open Multi-Processing (OMP) for the parallelization of all computational loops within each component's individual calculation. Communication between the three independent computations is needed only once per iteration. Once each component's 3D FFT is completed, the results of each must be transmitted to each of the other nodes for use in its application of its component's wavenumber response for the pseudo-spectral analog of the spatial derivatives of equation 3. After this single communication, all other computations continue in parallel. Table 1 shows a schematic of the program flow of the parallel implementation.

In general, the computational complexity can be determined by the time of the 3D FFT employed. Three forward FFTs are required, one for each component, so that the pseudo-spectral wave number operators can be applied. Three inverse 3D FFTs are then performed to return to the space domain. Since all other compute times are small compared with the FFT, the timing can be estimated as the time required to complete six 3D FFTs for the size of the problem. If a parallel implementation like that described here is used, the timing is reduced to two 3D FFTs plus the time required to exchange the three components' wave fields.

For the spatial derivatives we chose the pseudo-spectral method without grid staggering. This works well for many problems, but for some cases more accurate alternatives can be used without changing the main subject of this paper , which is the use of the rapid expansion method for the time evolution. Fornberg (1986), Canuto et al. (1987) and Carcione (1999, 2001, 2006) discuss the use of staggered grids with the pseudo-spectral method and of course the finite difference method can also be employed (Mittet, 2010), with and without staggered grids, to compute the required spatial derivatives. Any of these methods can be employed without affecting the parallel implementation scheme outlined here, or the use of the rapid expansion

method for the time marching. The final accuracy of the simulation will depend on the spatial variability of the model, the numerical scheme selected for the estimation of the spatial derivatives and the explicit time marching employed.

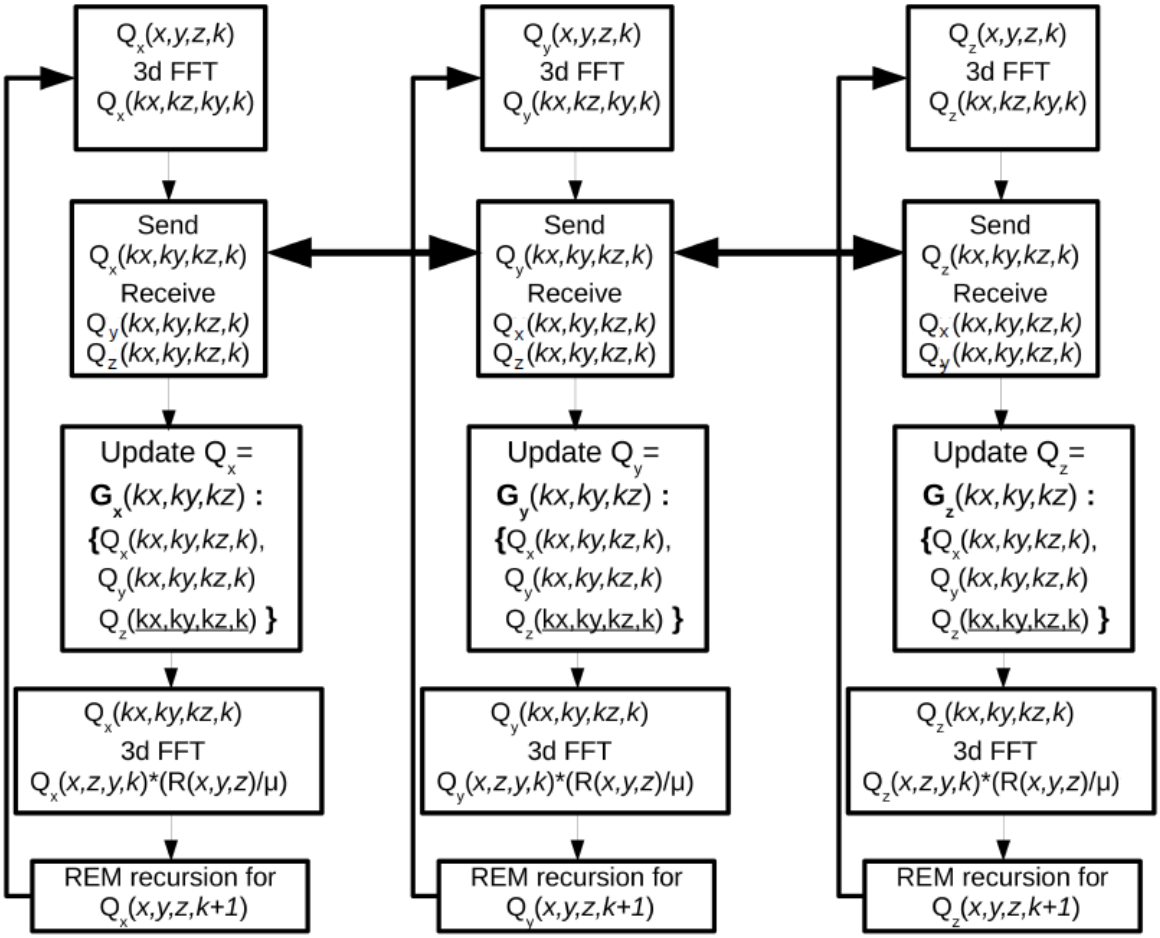

Table 1. Computation of each component of the E field proceeds in parallel using MPI as indicated by the three program units. Communication of intermediate results between program units (as schematically indicated by the horizontal arrows) occurs only once per polynomial evaluation after the 3D FFT of each component. The G matrix operator which is specific to each component but requires all 3 E fields can then be applied in parallel to update its E-field component. This operator as well as the FFT's are also computed within each program unit in parallel using OMP. After the G operator is applied, the inverse 3D FFT is performed, the spatial operator is applied, and the REM recursion is then used to get the next Chebyshev polynomial.

EXAMPLES

Analytic impulsive dipole source response test

We first report on the pseudo-spectral rapid expansion 3-D EM forward modeling by comparing results of the modeling with the analytic solution for a full-space. No filtering is applied in time or space. The dipole source generates a field everywhere in the model after a small finite time and this serves as the initial condition. The dipole source can be placed anywhere in the model, but we have found that it is important not to put the center of the E_y or E_z components of the source on an exact y or z grid node as this introduces zeros along lines of nodes in the model and causes ringing in the propagating field. Consequently, the impulsive dipole source was placed close to the center of a 100 x 100 x 100 cube with a grid spacing of 20 m in all directions. To avoid complications with any type of numerical boundary condition, we simply extended this cube to 128 x 128 x 128 which also is appropriate for the FFT. The additional 14 samples on each edge of the original cube proved adequate to avoid nearly all edge effects except for the very latest arrival times near the edge of the model as pointed out below. For this full-space model an initial dipole field was calculated at a time $t_0 = 0.00125$ s, and the field was then propagated. The resulting field was then compared with the analytic response for all three components of the electric field for one receiver along a line above the source and then for the E_x field with decreasing distance from the source.

Figure 1 shows the 1 ohm-m full space model. The source was placed close to the middle of the model at (1005, 1005, 1005), with the spatial units in meters.

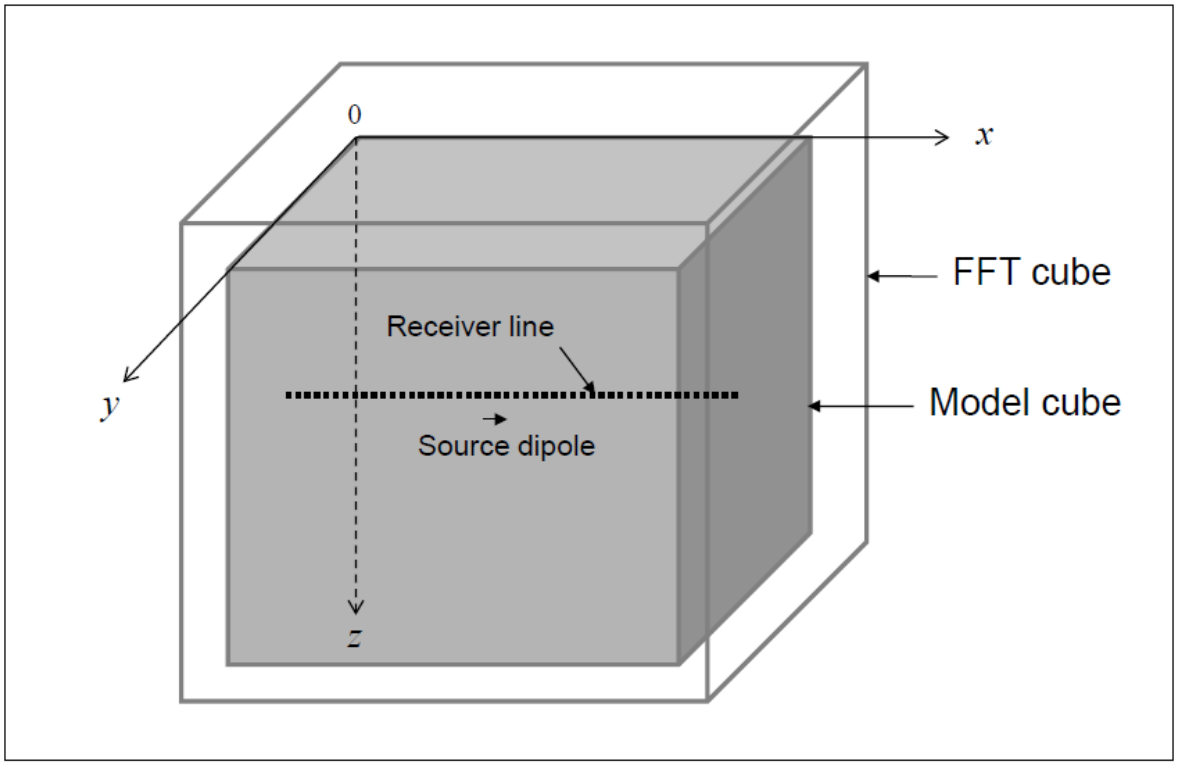

Figure 1 Full-space model cube 100 x 100 x 100 grid points within an FFT cube 128 x 128 x 128 samples. The origin of the Cartesian coordinates is at one corner of the model cube; axes are coincident with three edges, as shown. Spatial sampling is $\Delta x = \Delta y = \Delta z = 20$ m. The 1 amp-m x-directed source dipole is at (1010, 1010, 1010); that is, not at a grid point. Receivers are placed along a line parallel to the x-axis at $y = 1000$ m, $z = 900$ m.

We generated the impulse response of the 1 ohm-m full space for times that are consistent with our spatial sampling. First, the initial field of an impulsive dipole source was generated at a time

$$t_0 \approx 2.5\mu\sigma(\Delta l)^2 , \tag{14}$$

where $\mu = 4\pi 10^{-7}$, $\sigma = 1$ Sm^{-1} in this case, and Δl is the smallest of Δx, Δy, and Δz; that is, $\Delta l = 10$m in this case. Equation 14 is a rule of thumb we have found that gives reasonable answers. For these parameters $t_0 = 4\pi 10^{-4}$ s; we used $t_0 = 0.00125$ s.

The field at (x,y,z) at time t due to an impulsive x-directed current dipole source at (x_s, y_s, z_s) can be derived in a number of ways and is, for example, the time derivative of the step function response derived by Ward and Hohmann (1987) and given by

$$\mathbf{E_I} = \frac{D}{8}\sqrt{\frac{\sigma\mu^3}{\pi^3 t^5}}\exp\left(-\frac{\mu\sigma r^2}{4t}\right)\left[\left(1-\frac{\mu\sigma}{4t}\left((y-y_s)^2+(z-z_s)^2\right)\right)\mathbf{u_x}\right.$$
$$\left. + \frac{\mu\sigma(x-x_s)(y-y_s)}{4t}\mathbf{u_y} + \frac{\mu\sigma(x-x_s)(z-z_s)}{4t}\mathbf{u_z}\right] \tag{15}$$

where D is the dipole moment, $\mathbf{u}_x$, $\mathbf{u}_y$, and $\mathbf{u}_z$ are unit vectors, and

$$r = ((x-x_s)^2+(y-y_s)^2+(z-z_s)^2)^{1/2} . \tag{18}$$

These formulae were used to calculate the initial field at $t = t_0$ at all grid points in the model. For a 1 amp-m source D = 1 amp-m. Once the model and source position are defined, the only free parameter is t_0.

The initial field was then propagated using the Chebyshev polynomial recursive pseudo-spectral program. Only the number of iterations in the recursion, which is determined by the maximum response time, remains to be determined. Carcione derived a formula (Carcione, 2006, equation 37), for the number of Chebyshev terms required for the 2D problem that included a factor β that should be between 5 and 6. We have found that 6 is sufficient.

The pseudo-spectral fields at each receiver position were calculated for 150 time samples with a sample interval of $\Delta t = t_0 = 1.25$ ms. The analytic signal at each receiver position was evaluated at the same times using equation 17. The calculations, shown in Figures 2, 3 and 4, took about 17 minutes on a single-core desktop computer.

First, our results are compared for two receiver positions at $z = 900$ m in Figure 2. Their coordinates are (500, 1000, 900) m and (1520, 1000, 900) m. These positions are symmetric about the *x*-coordinate of the source, but not quite symmetric for the *y* and *z* coordinates, because the source is not at a node. The synthetic and analytic signals should be the same and Figure 2 shows no observable difference. E_x should be symmetrical and it is. E_y and E_z should be almost completely anti-symmetrical and they are. We note that the E_y signal is an order of magnitude smaller than E_z and two orders of magnitude smaller than E_x.

Next, we look at how the E_x response varies with distance from the source. This test shows responses from close to the side of the box, x = 100 m, and almost to the centre, x = 1000 m, in steps of 100 m. Because of the established symmetry it is not necessary to show the other half of the line. The results for x = 100 m to x = 600 m are shown in Figure 3 and for x = 700 m to x = 1000 m in Figure 4. Almost all the plots are exactly right. Figure 5 shows the relative percentage error for three offsets: x = 100 m (offset = 900 m), x = 500 m (offset = 500 m), x = 900 m (offset = 100 m).

For x = 100 m (offset = 900 m) a small difference between the synthetic and analytic solutions is seen in Figure 3 at late times. Figure 5 shows that the error is about 2% at 15 ms, decreases to a minimum of about 0.002 % at 60 ms and increases steadily thereafter to about 5 % at 200 ms. We attribute this error to bounce back into the grid from the boundary. For x = 200 m (offset = 800 m) the error is just perceptible in Figure 3 at late times. For x = 300 m to x = 1000 m (offsets from 700 m to 50 m), the results appear perfect in Figures 3 and 4. Figure 5 shows the relative error at x = 500 m to be less than 0.1 % for most times, the maximum error being less than 1 % for a few milliseconds at around 10 ms. At x = 900 m the error is less than 0.01 % for all times to 200 ms. For comparison purposes we did not use any numerical boundary conditions. The use of perfectly matched layers (PML) (Berenger, 1994; Chen, Chew and Oristaglio, 1997) should improve the results shown here near the edge of the cube and is appropriate for more general modeling applications.

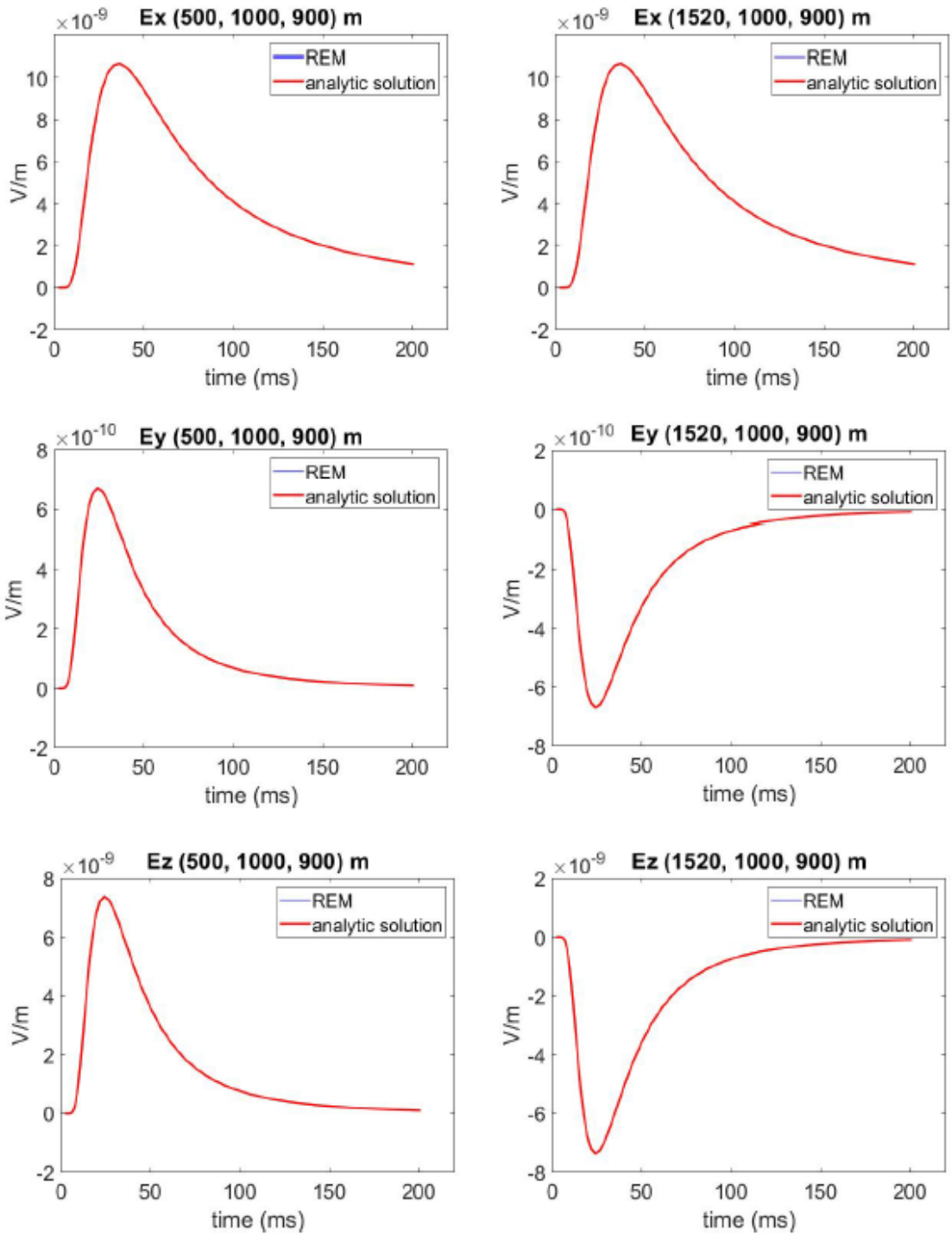

Figure 2 Comparison of pseudo-spectral (blue) and analytic (red) responses for E_x, E_y, and E_z components at (50, 1000, 900) m on the left and (1520, 1000, 900) m on the right.

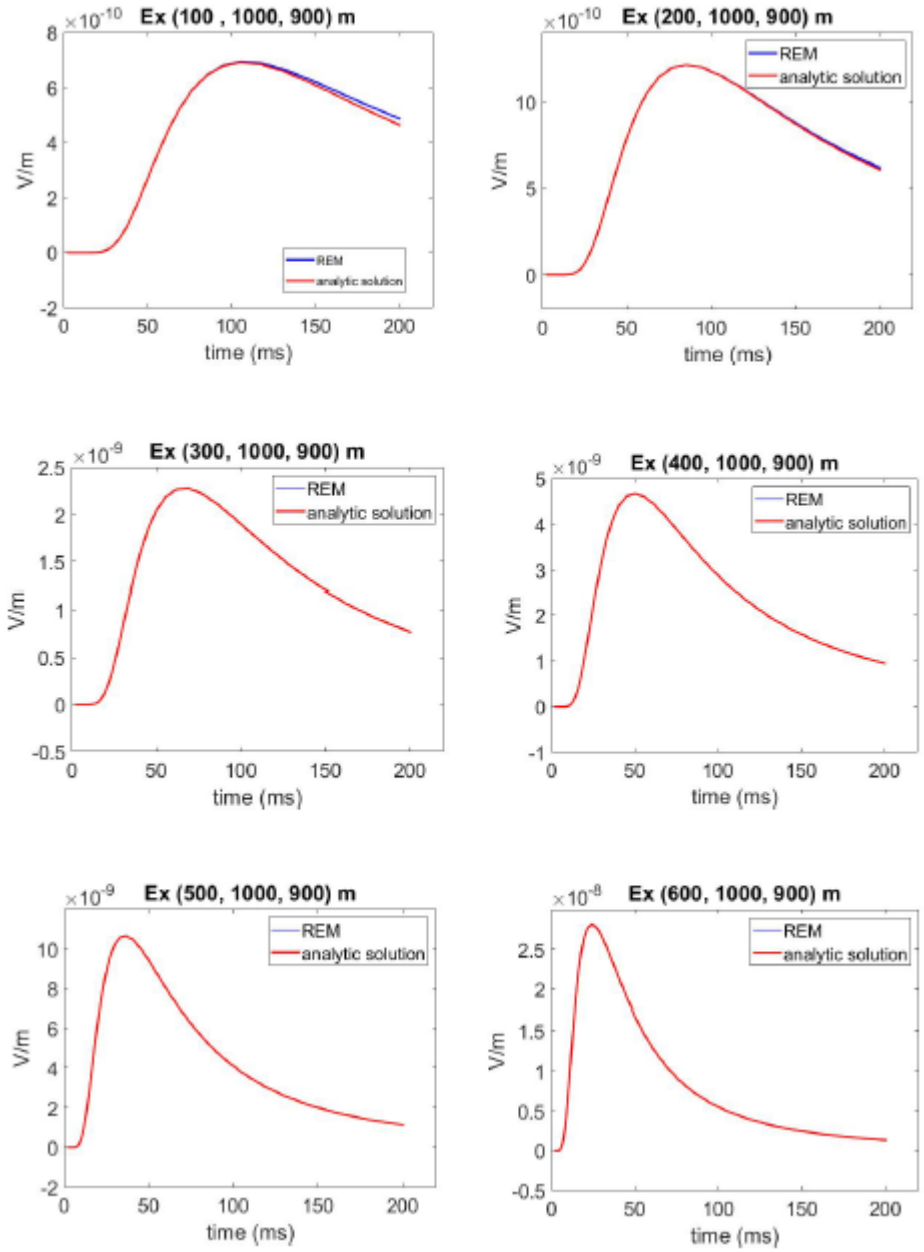

Figure 3 Comparison of pseudo-spectral (blue) and analytic (red) responses for E_x for x = 100 m, 200 m, 300 m, 400 m, 500 m, 600 m; y = 1000 m; z = 900 m.

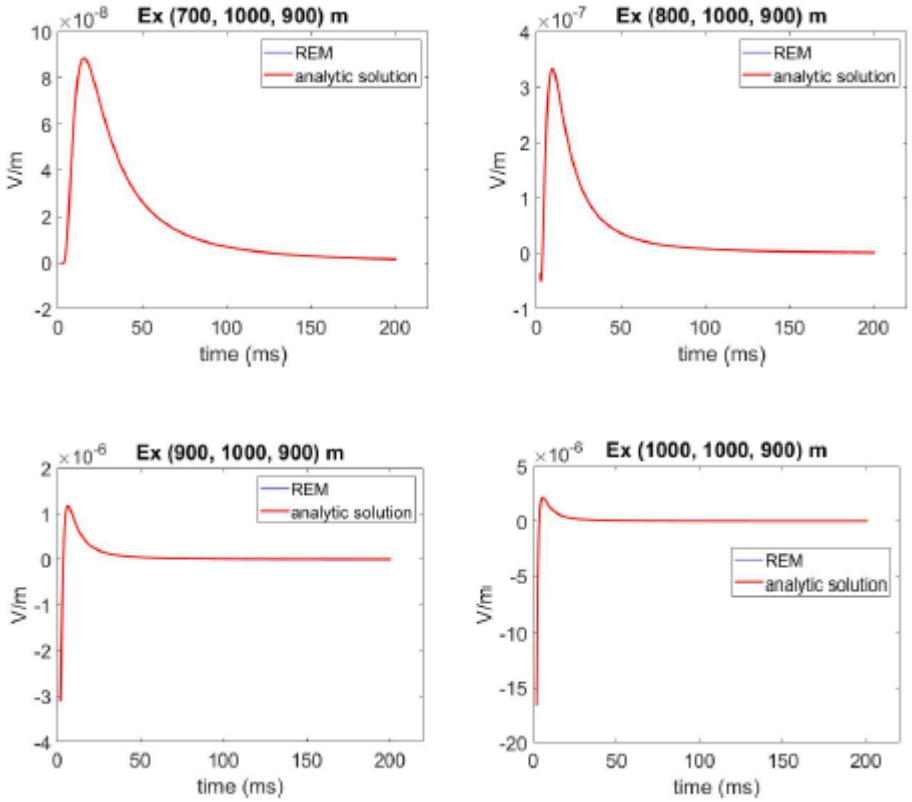

Figure 4 Comparison of pseudo-spectral (black) and analytic (red) responses for E_x for x = 700 m, 800 m, 900 m, 1000 m; y = 1000 m; z = 900 m.

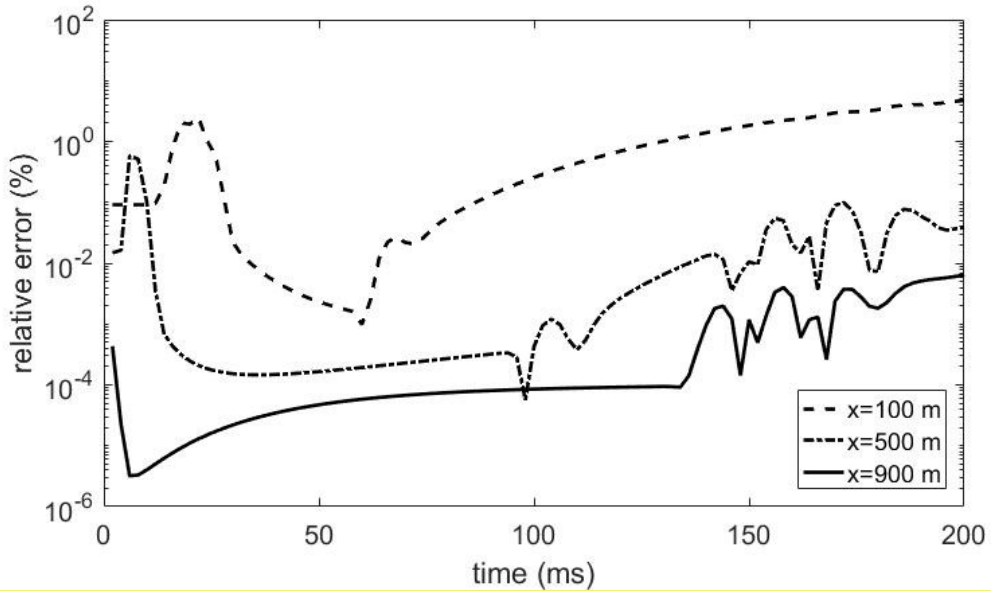

Figure 5 Relative error plot for E_x for x = 100 m, 500 m, 900 m; y = 1000 m; z = 900 m.

Our comparison of the pseudo-spectral rapid expansion 3-D EM forward modeling code with the analytic solution for a full-space indicates that the method is numerically very accurate and produces synthetic data that match the analytic solution almost exactly in the main part of the model. There is no numerical dispersion and we have applied no filtering in time or space. Using a better boundary condition should eliminate the small errors that are observed near the boundaries of the computational cube.

1D Example

Next we compare a reflectivity method (Slob et al., 2010) using the program EMmod described in Hunziker et al. (2015) to the pseudo-spectral REM method. The model is defined on a 400 x 400 x 400 computational grid with a sampling interval of 10 m in each direction. The first 220 samples in depth (2200 m) has a resistivity of 0.3333 ohm-m. From samples 221 to 300 (2210 m to 3000 m) the resistivity increases to 1.0 ohm-m and from sample 301 to 400 (3010 m to 4000 m) the resistivity again increases to 2.0 ohm-m.

The source was an injected analytic Ex dipole at 0.5 ms located almost at the center of the grid, but evaluated for an origin of 2005 m, 2005 m, 2005 m. The receivers were located at all x grid positions and for a y line at 2000 m. The receivers were at a depth of 2100 m, placing them about midway in depth between the source and first reflector. Based on this geometry there should be a direct wave, reflections from the first and second interfaces, and refractions.

Figure 6 shows snap shots for the x (upper) and z (lower) components of the Chebyshev polynomials, k, for the center line, y = 2000 m of the 3D computational volume. These snap shots were selected because: (1) the first, at k = 200, shows the initial interaction with the first reflector; (2) the second, at k = 400, shows this reflection going up towards the receiving array;

(3) the third, at k = 600, shows it continuing towards the surface; (4) the fourth, at k = 800, shows the reflection from the second interface. Note the polarity differences between the x and z components.

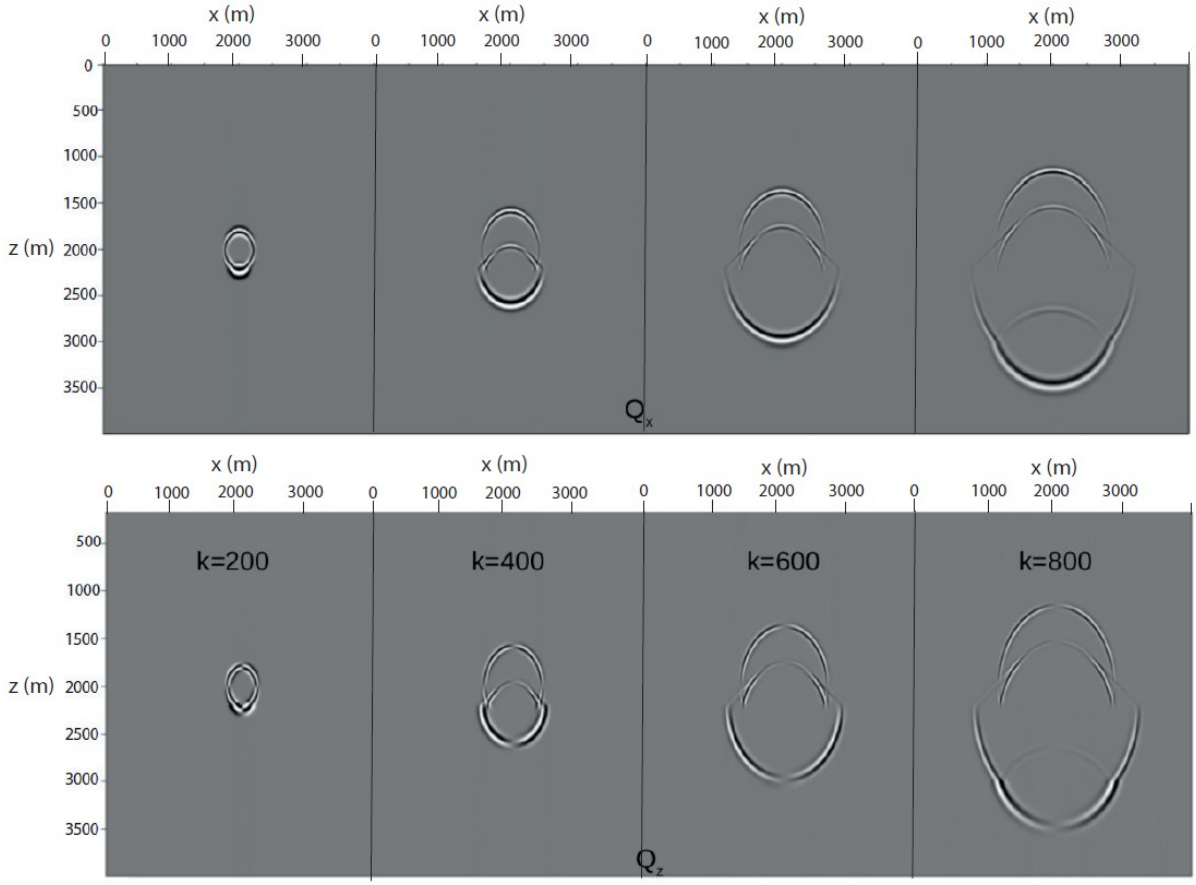

Figure 6. Snapshots of the x (upper) and z (lower) components of the Chebyshev polynomials, k = 200, 400, 600 and 800. Increasing k shows the evolution of the electric wave field components and their interactions with the 1st and 2nd reflectors. Note also the polarity of the z component.

Combining equations 3, 6 and 9, the Chebyshev recursion for generating the new polynomials, Q_k, from those previously calculated may be rewritten for $k > 1$ as

$$\frac{1}{\Delta p^2}\left[\mathbf{Q}_{k+1} - 2\mathbf{Q}_k + \mathbf{Q}_{k-1}\right] = -v^2 \nabla \times \nabla \times \mathbf{Q}_k \,. \tag{17}$$

This is a discrete wave equation, where $v^2 = 1/(\mu\sigma)$. The equivalent of Δt, the usual time variable, is Δp, which we define as $\Delta p = \sqrt{2/b}$, where b is defined in equation 12, and note that $t_k = [(k-1)\Delta p]^2$ has units of seconds. This defines a nonlinear time grid for the linear Δp grid associated with each Chebyshev polynomial Q_k. This result explains the wave-like character of the polynomials in the snapshots shown and the recorded response at the receivers.

We collected the samples of the Chebyshev polynomial for each k at the receivers and display them in Figure 7 for positive offsets of 0 to 2000 m. Note the vertical axis is polynomial number k. We can see the direct wave, reflections from the two interfaces, and what appears to be a refraction. Since this is a 1D model, the negative source-receiver offset data are identical with the positive offset data for the x component.

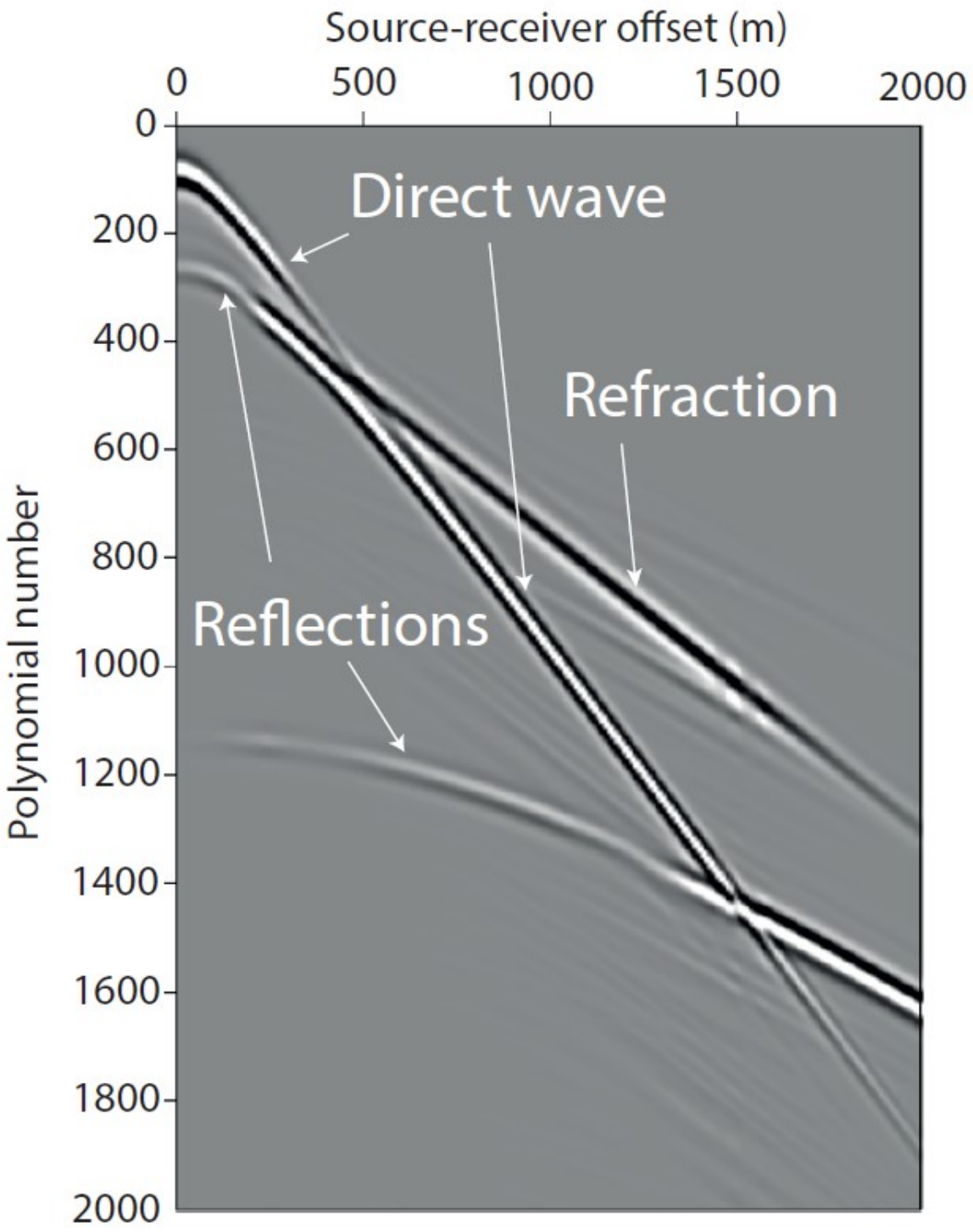

Figure 7. Chebyshev polynomials for the *x* component of the electric field shown for source-receiver offsets of 0 to 2000 m. You can easily identify the direct arrival and reflections from the first and second interfaces. Also visible is a refraction from the second layer. No filtering of any kind was applied to the data and the data were scaled to the maximum amplitude value for display purposes.

In Figure 8 we show a plot of a reflectivity method (a) and the method presented here (b) for the 1D earth model and offsets from 0 to 1000 m shown every 100 m or 10th offset. For comparison, the amplitudes of each trace were normalized to the maximum. No other filtering was applied to the data. The data in Figure 8(b) should be compared to the first half of Figure 7, which are the equivalent Chebyshev polynomials (but for every offset recorded). It is clear from the snapshots and the comparison of Figures 7 and 8 that the role of the modified Bessel function is to turn the wave-like response of the Chebyshev polynomials into the expected diffusive response of the **E** fields.

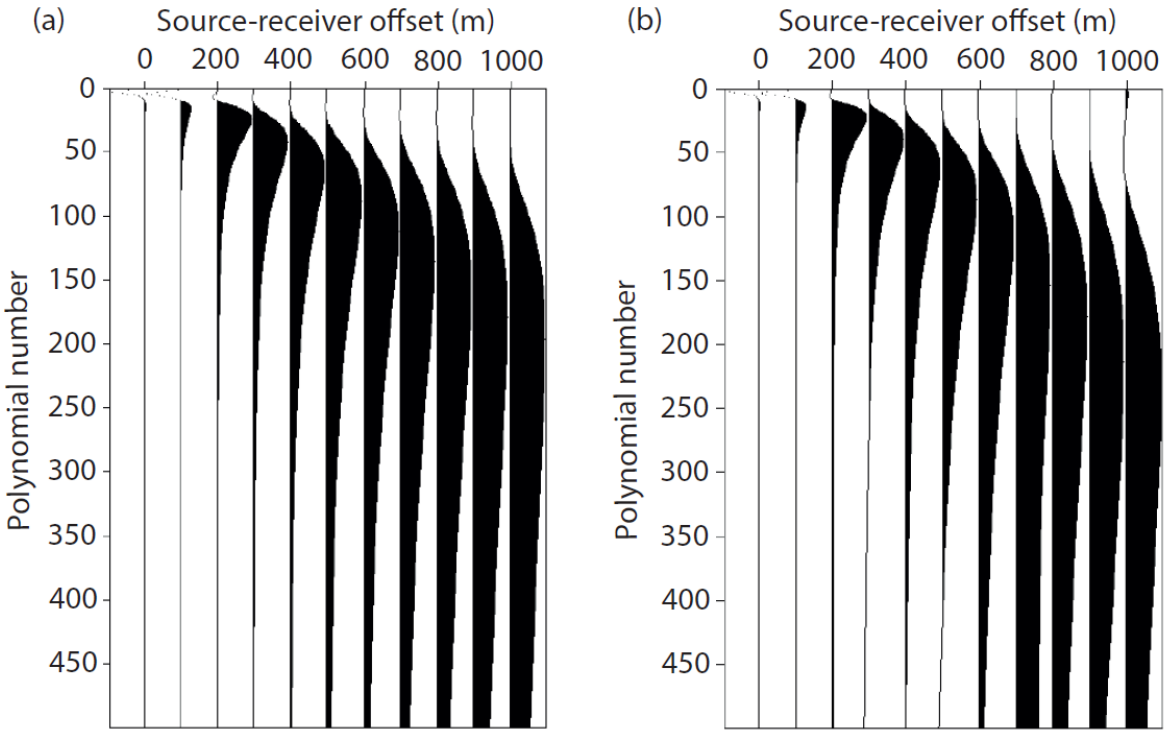

Figure 8. Variable area plot of the E_x simulated data with increasing x offset along the source y = 2000 m line: (a) the reflectivity results; (b) the results from the pseudo-spectral REM method. Every 10th receiver is shown, so the offsets range from 0 to 1000 m. The results are very similar except for the latest arrival times where small differences occur.

We have shown that the Chebyshev algorithm generates a series of discrete fields that satisfy the discrete wave equation in which the discrete time-like variable has a sampling interval Δp with dimensions of square-root of time and propagation velocity $1/\sqrt{\mu\sigma}$ with dimensions of length divided by square-root of time. Our work is clearly related to the work of Lee et al. (1989), who presented a continuous integral representation to relate the electromagnetic diffusion response to a fictitious wave field that satisfies the wave equation with the same dimensions for the time-like variable and velocity, respectively.

3D Example

We next illustrate the pseudo-spectral REM computational method for a 3D model. The model is defined on the same 400 x 400 x 400 computational grid with a sampling interval of 10 m in each direction.

The basic model was the same as our 1D case: the first 220 samples in depth (2200 m) had a resistivity of 0.3333 ohm-m; from samples 221 to 300 (2210m to 3000m) the resistivity increased to 1.0 ohm-m; and from sample 301 to 400 (3010m to 4000m) the resistivity again increased to 2.0 ohm-m. We then introduced a fault block of 50m and removed the second layer from the uplifted fault block. The fault block extends from samples y = 191 to 210 (1910 m to 2100 m) and from sample 161 to 190 (1610 m to 1900 m) in x. Figure 9 shows the model geometry using two cross-sections. Figure 9a shows all x for y = 2000 m and Figure 9b shows all y for x = 1850 m. Thus the 50m uplift is an area of 200m in y by 300m in x.

The source and receiver geometry were the same as for the 1D example; that is, the source was an injected analytic $\mathbf{E}_x$ dipole at 0.5 ms located almost at the center of the grid (200, 200, 200), but at (2005m, 2005m, 2005m) instead. The receivers were located for all x and y grid points in depth at grid point 210 or 2100m.

Based on this geometry there should be a direct wave and reflections from the first and second interfaces. But the results of the 3D geometry should show a more complicated set of arrivals, including diffractions and offsets in the arrival times and offsets due to the fault block.

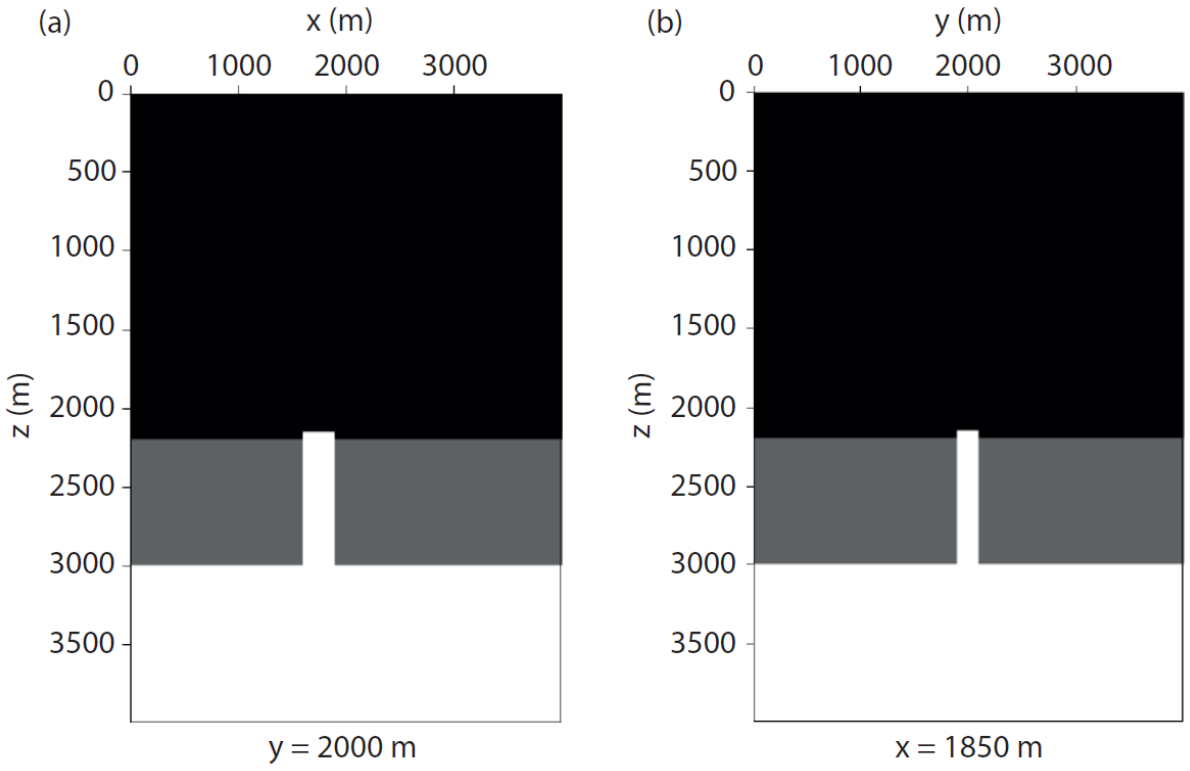

Figure 9. (a) Line at y = 2000 m for all x; (b) line at x = 1850 m for all y. Resistivities from the top down are 0.33333, 1.0 and 2.0 ohm-m, respectively.

Figure 10 shows snapshots for (a) the x-component and (b) the z-component Chebyshev polynomials, k, for the center line, y = 2000 m of the 3D computational volume. These snap shots should be compared with the 1D case, shown in Figure 5. They contain significant differences due to the interactions with the 3D structure.

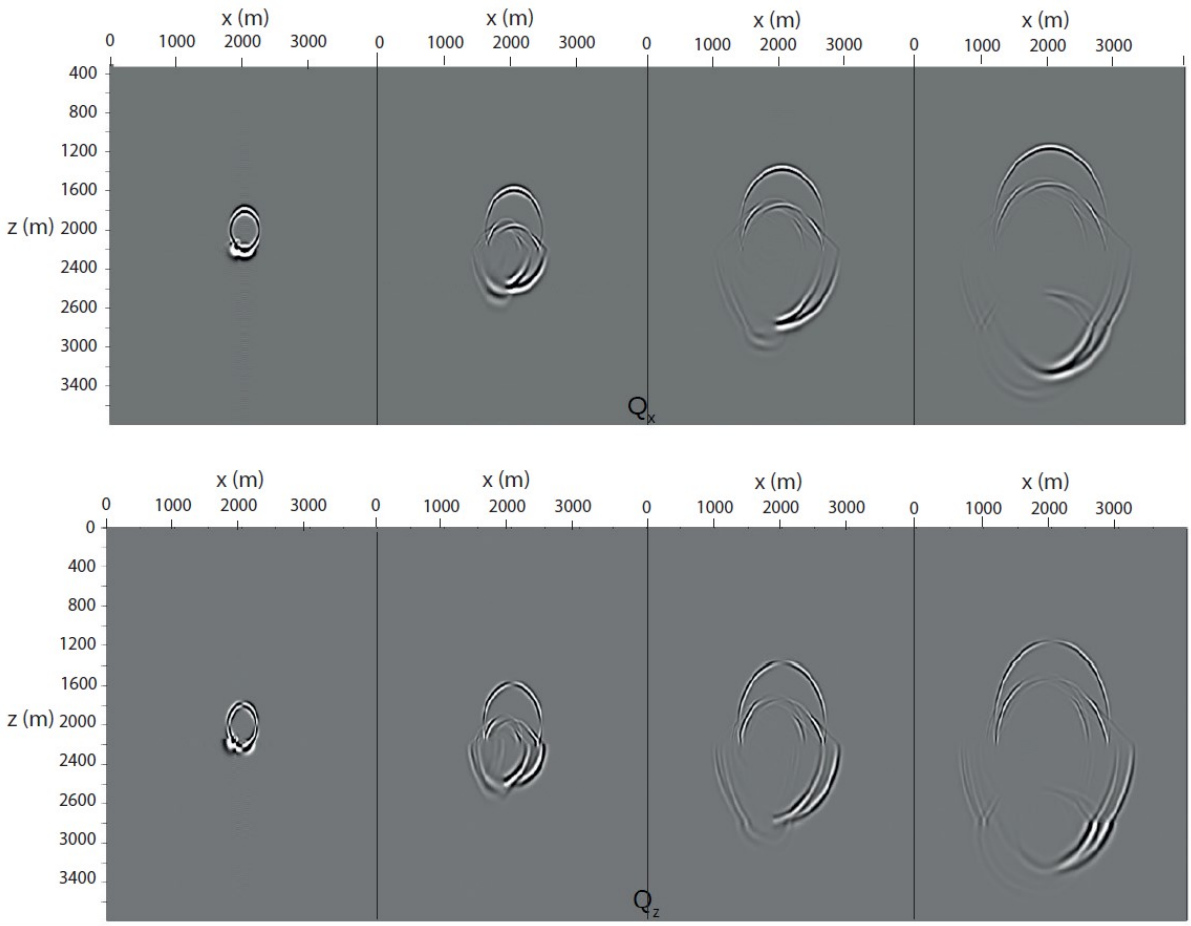

Figure 10. Snap shots for the *x*-component (upper) and *z*-component (lower) Chebyshev polynomials, *k*, for the center line, *y* = 2000 m of the 3D computational volume.

Figure 11 shows the E_x data for the 3D example. The vertical axis is in terms of the polynomial number, *k*. (Polynomials for *k* = 1 to 2000 are shown, which in time is the range 0.0 to 17 s.) The horizontal scale ranges from 0 m to + 4000 m for each section, with mid-point of each section being the source location, that is, 2005 m. The data are scaled within each plot so the display is relative true amplitude. The data shown had a high cut at 95% of Nyquist and a three-trace mix was used to enhance the signal level at the far offsets and late times. A high gain was used with clipping so that even the much weaker late and far offset arrivals can be seen. The Chebyshev polynomials which were used in the integration are shown below the **E** fields. You can see that lateral changes in the intensity of the **E** fields can be related to the

character of the arrivals in the polynomials. We note that the 1D Ex (Figure 11a) is not quite symmetric because the source was at 2005 m in x and y.

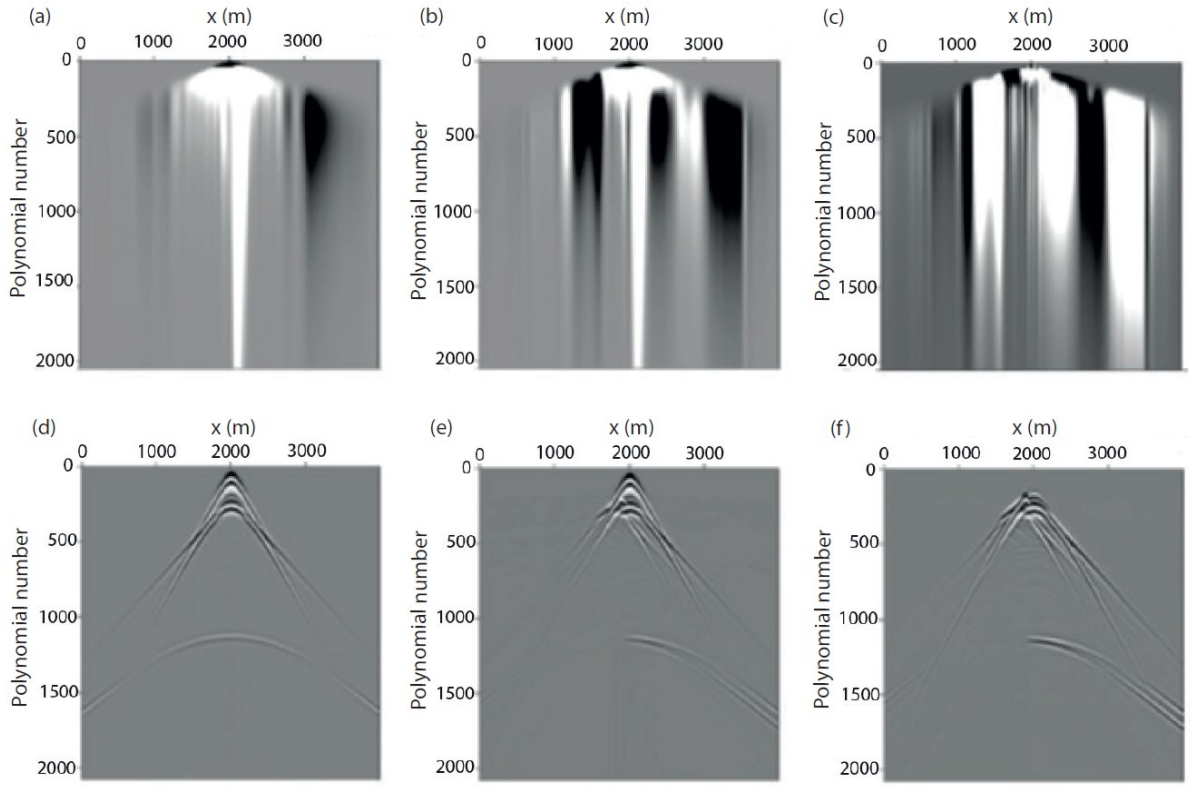

Figure 11 shows the E_x data (a, b, c) and Chebyshev polynomial data (d, e, f) data for the 1D example (a and d) and the 3D example (b and e). In c and f are the data that result when the response of the direct wave is removed from the 3D data. Horizontal scale is meters. Vertical scale is polynomial number.

Even though the Chebyshev polynomials show significant differences between the 3D and 1D cases as expected, the final resulting E_x field does not show the same level of detail. This we attribute to the strong influence of the early arrivals, the direct wave and, most likely, the reflection from the first layer, and how these large amplitudes are distributed during the integration with the modified Bessel function to produce the diffusion response.

In Figure 11, we evaluated the E_x field on the equivalent (or same) temporal grid as the polynomials. The early high amplitude arrivals in the recorded **E** fields are generally not of interest and can be categorized as coherent noise that, if removed, should reveal the underlying arrivals of interest. We can simply replace the model with a homogeneous half space with the

parameters of the first layer and run the 3D simulation to get the impulse responses at the receivers. These can then be removed to reveal the arrivals of interest. In our synthetic case, this was easily accomplished by simple subtraction of the computed impulse response from the data. In Figure 11 (c and f) we simply subtracted the impulse response which, for our deep water example, is the direct wave, to reveal the **E** fields associated with the sub seafloor structure of interest. For real data this can be cast as a well-constrained inverse problem, since the source and receiver geometry are known and their response calibrated. Also, the resistivity of the observation layer should be known approximately. In fact, this approach can be used to include the air wave for shallow water acquisition and even the response of the sea floor can be included, as its geometry is known and the only unknown is the resistivity just beneath the sea floor.

So we are suggesting that the initial processing should be to remove the effects of the direct wave, air wave and possibly the first reflector as a small inverse problem before further interpreting the data. (Very likely, the same strategy will have to be applied for each subsequent reflecting interface.)

In Figure 11 (d, e and f) the Chebyshev polynomials Q_x show significant differences for the three cases. First, significant changes are seen between the 1D (d) and 3D (e) cases. Second, we see in Figure 11(f) that the direct wave has been removed to reveal only the events of interest. It is clear from this example that it would be preferable to interpret the Chebyshev polynomials rather than the E data directly, as the primary events are easily recognized and resolved in time and space.

DISCUSSION

Other researchers have noted that a wave-like response can be developed for this diffusion problem, which promises to aid the modelling and interpretation of transient EM data. The

work of de Hoop (1996), using the time-Laplace representation, relates any time-domain electromagnetic diffusion field to an electromagnetic wavefield in a 'corresponding' configuration in which the electrical conductivity in the diffusive case is a positive scalar factor times the electrical permittivity in the wave-propagation case. Mittet (2010) uses the formulation of de Hoop, but uses Fourier transforms instead of Laplace transforms. In both these formulations the time axis in the fictitious wave domain retains the dimensions of time and velocity retains the dimensions of length/time. These two formulations are special cases and are not related to the waves we describe, which are the result of the Chebyshev expansion. Lee et al. (1989) make a transformation of variables in both the time domain and frequency domain and their resulting equations are a continuous analog of the discrete wave equation we obtain here. Further, their time-like variable and velocity have the same units that we have derived for the Chebyshev waves: $\sqrt{s}$ and m/$\sqrt{s}$, respectively. It remains to be shown that the integral transformation (equation 11) of Lee et al. (1989) and our summation with modified Bessel function weights are in fact the analog and discrete equivalents of each other. Further, whether we can recover the Q_k at the receivers and use these to process, image and interpret the data remains a topic for future consideration.

CONCLUSIONS

We have demonstrated that the new flexible 3D three-component full-bandwidth modeling method for transient CSEM data is accurate, by comparing it with the analytic response to a point dipole in a full space. Similar accuracy is obtained in comparisons with 1D modeling. The diffusive field is a weighted sum of Chebyshev polynomials, which exhibit a wave-like character and are very sensitive to small perturbations in the medium once the dominating effects of the direct wave (and, when appropriate, the air wave) have been removed.

The method we developed can be implemented in parallel at two levels. First, each component of the electric field can be computed independently and the updated **E**-field components exchanged only once per polynomial evaluation. Second, within each of these global processes, local parallelism is achieved over all computational loops. This implementation combined with parallel FFTs makes the method computationally feasible.

Our 3D example shows that the effects of the direct wave, air wave, etc., which should be known at least approximately, should be removed from the data before interpretation of the **E** fields can be expected to reveal interpretable differences. But most of all, it is very clear from all the examples that it would be easier to interpret and image the Chebyshev polynomials, Q_k, if they could be extracted from the recorded E data.

ACKNOWLEDGMENTS

We thank A. O. Daalhuis and J. Vanneste for helpful discussions, and A.O. Daalhuis in particular for help with equation 17. We thank Y. Liu for help with computing the examples in Figures 2-5. We thank assistant editor J. Shragge, reviewer R. Mittet, and two anonymous reviewers, who all provided very constructive comments and suggestions that greatly improved the paper.

DATA AND MATERIALS AVAILABILITY

The paper contains only synthetic data calculated using algorithms described in the paper or using published code, as detailed in the paper.

REFERENCES

Abramowitz, M. and I.A. Stegun, 1972, Handbook of mathematical functions: Dover Publications, Inc.

Anderson, C., and J. Mattsson, 2010, An integrated approach to marine electromagnetic surveying using a towed streamer and source, *First Break*, **28**, 5, 71-75.

Berenger, J.-P., 1994, A perfectly matched layer for absorption of electromagnetic waves: *Journal of Computational Physics*, Vol. **114**, 185-200.

Canuto C., M. Y. Hussaini, A. Quarteroni, and T. A. Zang, 1987, Spectral methods in fluid dynamics: Springer-Verlag New York, Inc.

Carcione, J. M., 1999, Staggered mesh for the anisotropic and viscoelastic wave equation: *Geophysics*, **64**, 1863-1866.

Carcione, J.M., 2001, Wave fields in real media: wave propagation in anisotropic anelastic and porous media, *in* Helbig, K. and S. Treitel, eds., Handbook of Geophysical Exploration, Vol. 31: Pergamon.

Carcione, J.M., 2006, A spectral numerical method for electromagnetic diffusion: *Geophysics*, 71, No.1, I1-I9.

Chen, Y. H., Chew, W. C., and Oristaglio, M. L., 1997, Application of perfectly matched layers to the transient modelling of subsurface EM problems: *Geophysics*, **62**, no 6, 1730-1736.

Cox, C. S., 1981, On the electrical conductivity of the oceanic lithosphere: *Physics of the Earth and Planetary Interiors*, **25**, 196–201.

Druskin, V and L. Knizhnerman, 1994, Spectral approach to solving three-dimensional Maxwell's diffusion equations in the time and frequency domains: *Radio Science*, **29**, 937-953.

Edwards, R.N., and A.D. Chave, 1986, A transient electric dipole - dipole method for mapping the conductivity of the sea floor: *Geophysics*, **51** , no. 4, 984-987.

Eidesmo, T., S. Ellingsrud, L. M. MacGregor, S. Constable, M. C. Sinha, S. Johanson, F. N. Kong, and H. Westerdahl, 2002, Sea bed logging (SBL), a new method for remote and direct identification of hydrocarbon filled layers in deepwater areas: *First Break*, **20**, 144–152.

Ellingsrud, S., T. Eidesmo, S. Johansen, M. C. Sinha, L. M. MacGregor, and S. Constable, 2002, Remote sensing of hydrocarbon layers by seabed logging (SBL):Results from a cruise offshore Angola: *The Leading Edge*, **21**, 972–982.

Fornberg, B., 1987, The pseudo-spectral method: Comparisons with finite differences for the elastic wave equation: *Geophysics*, **52**, No. 4, 483-501.

Fornberg, B., 1988, The pseudo-spectral method: Accurate representation of interfaces in elastic wave calculations: *Geophysics*, **53**, No. 5, 625-637.

Hesthammer, J., A. Stefatos, M. Boulaenko, S. Fanavoll, J. Danielsen, 2010, CSEM performance in light of well results: *The Leading Edge*, **29**, 29-34.

Hunziker, J., Thorbecke, J., and Slob, E., 2015, The electromagnetic response in a layered vertical transverse isotropic medium: A new look at an old problem: *Geophysics*, **80**, no 1, F1-F18.

Kosloff, D., Filho, A. Q., Tessmer, E., and Behle, A., 1989, Numerical solution of the acoustic and elastic wave equations by a new rapid expansion method: *Geophysical Prospecting*, **37**, 383-394.

Lee, K.H., G. Liu and H. F. Morrison, 1989, A new approach to modelling the electromagnetic response of conductive media: *Geophysics*, **54**, 1180-1192.

Mittet, R., 2010, High-order finite-difference simulations of marine CSEM surveys using a correspondence principle for wave and diffusion fields: *Geophysics*, 75, No. 1, F33-F50.

Pestana, R.C. and P.L. Stoffa, 2010, Time evolution of the wave equation using rapid expansion method: *Geophysics*, 75, No.4, T121-T131.

Schwalenberg, K., E. Willoughby, R. Mir and R. N. Edwards, 2005, Marine gas hydrate electromagnetic signatures in Cascadia and their correlation with seismic blank zones, *First Break*, 23 ,4, 57-64.

Sinha, M. C., P. D. Patel, M. J. Unsworth, T. R. E. Owen, and M. R. J. Mac-Cormack, 1990, An active source EM sounding system for marine use: *Marine Geophysical Research*, **12**, 59–68.

Slob, E., J. Hunziker and W. A. Mulder, 2010, Green's tensors for the diffusive electric field in a VTI half-space: *Progress in Electromagnetics Research*, **107**, 1-20.

Tal-Ezer H., 1986, Spectral methods in time for hyperbolic problems: SIAM Journal of Numerical Analysis, **23**, 11-26.

Tal-Ezer H., 1989, Spectral methods in time for parabolic problems: SIAM Journal of Numerical Analysis, **26**, 1-11.

Ward, S. H. and G.W. Hohmann, 1987, Electromagnetic theory for geophysical applications, *in* Nabighian, M.N., 1987, Electromagnetic Methods in Applied Geophysics, Vol. 1, Society of Exploration Geophysicists, Tulsa, U.S.A.

Wright, D., A. Ziolkowski, and B. Hobbs, 2002, Hydrocarbon detection and monitoring with a multicomponent electromagnetic survey: The Leading Edge, **21**, No. 9, 852-864.

Ziolkowski, A., B. Hobbs, and D. Wright, 2007, Multitransient electromagnetic demonstration survey in France: Geophysics, **72,** No. 4, F197-F209.

Ziolkowski, A., D. Wright, G. Hall, and C. Clarke, 2008, Successful transient EM survey in the North Sea at 100 m water depth: 78th Annual International Meeting, SEG, Expanded Abstracts, 667-671.

Ziolkowski, A., R. Parr, D. Wright, V. Nockles, C. Limond, E. Morris, and J. Linfoot, 2010, Multi-transient electromagnetic repeatability experiment over the North Sea Harding Field: Geophysical Prospecting, **58**, 1159-1176.